Feasibility of Low-Power One-Way Travel-Time Inverted Ultra-Short Baseline Navigation

Michael V. Jakuba*, James C. Kinsey*, James W. Partan* and Sarah E. Webster†
*Woods Hole Oceanographic Institution, Woods Hole, MA USA
†Applied Physics Laboratory, University of Washington, Seattle, WA USA

***Abstract*—Recent and underway development efforts promise to deliver long endurance and deep-diving autonomous underwater vehicles with the potential to persistently observe the deep (6000 m) ocean interior and sea floor over time scales of months to years. These assets and their shallow-diving (<1000 m) predecessors navigate primarily by dead-reckoning between surfacing for GPS fixes, a paradigm that precludes their use in missions where science objectives call for precise navigation deep in the water column or near the deep sea floor. Coupled with a single autonomous surface vessel, one-way travel time inverted ultra-short baseline positioning (OWTT-iUSBL) offers a compelling, but presently unrealized, alternative to infrastructure-intensive external acoustic aiding. Such systems could provide navigation aiding to multiple underwater vehicles while retaining a level of autonomy and endurance for the system as a whole comparable to that of a solitary vehicle.**

While the concept of OWTT-iUSBL is not new, we argue that the maturity of acoustic modem technology combined with the emergence of very low-power precision timing and attitude sensors will make it possible to deploy OWTT-iUSBL systems on low-power underwater vehicles in the near term. This paper presents two analyses in support of this conjecture. First, we discuss the factors that govern the achievable accuracy of OWTT-iUSBL navigation and present single-fix error budgets for specific system configurations using representative commercially-available components. Second, we consider the impact of a specific low-power configuration on the endurance of a deep-profiling autonomous underwater glider. Our analyses suggest that a practically realizable OWTT-iUSBL system could provide navigational accuracy 1–2 orders of magnitude superior to that presently achievable using periodic ascents to acquire global positioning system (GPS), and, for sufficiently deep deployments, actually yield more near-bottom data despite reducing overall vehicle endurance.

I. Introduction

Technological developments over the past two decades have provided oceanographers with an impressive array of autonomous underwater vehicles, including autonomous underwater gliders (AUGs) [1], [2], [3], autonomous underwater vehicles (AUVs) [4], [5], [6], [7], [8], [9], and long-range AUVs (LRAUVs) [10], [11]. Collectively these vehicles provide a valuable *short-duration* (hours to days) observational capability throughout most of the water column (e.g., [12]), and valuable *long-duration* (weeks to months) observational capability in the upper thousand meters of the ocean (e.g., [13], [14]).

The recent emergence of long-endurance deep-diving (6000 m) vehicles [15], [16] challenges existing operational paradigms and provides new capabilities for persistently observing the deep ocean interior. However, navigation remains a challenge. While the navigation precision attainable by these assets is adequate to study near-surface and meso-scale oceanographic processes, current practice relies on regular access to the global positioning system (GPS). Thus the degradation in navigation resulting from extended time spent underwater precludes missions where navigational accuracy is critical, such as studying near-bottom processes ranging from localized deep flows around seamounts and sills to seafloor biogeography around hydrothermal vent sites. Fully realizing the potential of this new class of subsea assets will require innovations in low-power, high-precision navigation.

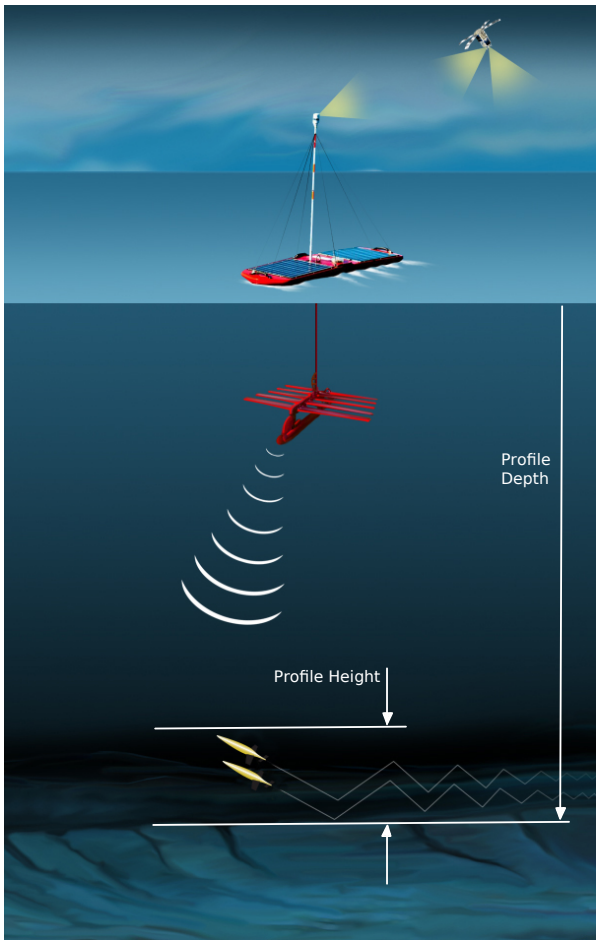

Fig. 1. Conceptual image of a possible OWTT-iUSBL system showing an ASV providing acoustic range and position information to a pair of AUGs. Our definitions of profile depth and height are also illustrated.

978-0-933957-43-5 ©2015 MTS

This paper considers one promising possibility (Fig. 1): one-way travel-time inverted ultra short baseline acoustic positioning (OWTT-iUSBL). We contend that OWTT-iUSBL, discussed in more detail in Section III, has the potential to overcome the existing obstacles of size, cost and power that preclude routine accurate externally-aided navigation in the ocean interior. We consider a notional system designed specifically to provide low-power geo-referenced acoustic positioning for a fleet of AUGs or LRAUVs when coupled with a modest ASV or other platform with access to precise position information (i.e. GPS). We present two analyses that demonstrate the potential benefits of OWTT-iUSBL. The first analysis (Section V) investigates the accuracy of this navigation system including dependencies on vehicle attitude sensors and alignment error. Vehicle attitude sensors range from highly accurate but expensive and power consumptive inertial navigation systems (INSs) found on large AUVs to low-cost, low-power micro-electrical-mechanical systems (MEMS) compasses found on gliders. The second analysis (Section VI) focuses on the effects of increased power consumption of a notional system on glider mission endurance and its impact on the volume of data collected.

II. Background

Because of disparities in size, available energy, cost, and operating domains, the navigation solutions employed by underwater robots vary enormously. High-power propeller-driven survey AUVs typically use Doppler velocity logs (DVLs) and INSs combined with external position measurements (e.g., ultra-short-baseline (USBL) or long-baseline (LBL)), while AUGs, which must use low-power sensors, typically depend on surface GPS measurements and suffer more rapidly degraded navigational accuracy while submerged. In a few cases, AUGs have been aided by acoustic means, when overlying ice and/or sustained monitoring activity justified the logistical overhead of permanent mooring-based ([17]) or semi-permanent ice-tethered ([18]) acoustic navigation infrastructure.

Conventional range measurements are based on the two-way acoustic travel time between the vehicle and sources. The use of one-way travel time (OWTT) methods eliminates the need for the receiver to transmit, instead enabling the receiver (e.g., the vehicle) to estimate ranges based on the one-way travel time of acoustic modem data packets that contain the data packet time of origin as well as the position of the transmitting source [19].

A further reduction in the overhead of range-aided navigation is the use of only a single acoustic source. Experiments by the authors [20], [21] and others [22] have demonstrated the feasibility single-source range-aided navigation. While this method enables new paradigms for operating AUVs, such as multi-vehicle extended duration missions, it suffers from two deficiencies: *(1)* acoustic data must be accrued over time and fused with dead-reckoned odometry (e.g., DVL/INS) and *(2)* range estimates from a variety of relative bearings between the source and the receiver must be attained to provide an suitable navigation fix [23], [24], [25], [26]. This is a challenge in deep water because large distances must be traversed to create significant changes in relative bearing.

In contrast, a USBL system requires bi-directional ranging but provides a full navigation fix from a single source. A receiver array resides on a surface vessel so that the range and relative azimuth and elevation can be fused with the location of the ship (known from GPS measurements). The underwater vehicle must expend energy to reply to each interrogation from the surface, and coded messages or other means of sharing the acoustic channel must be used to differentiate interrogations and replies from multiple vehicles, limiting scalability.

Similar in concept to standard USBL systems, an inverted (iUSBL) system architecture inverts the role of the surface vessel and underwater vehicle such that the acoustic cycle originates subsea rather than on the surface vessel. The surface vessel replies to each interrogation with a message that includes its position. The underwater vehicle computes the range, azimuth and elevation to the surface vessel upon receipt. Previous work includes efforts to develop and field iUSBL systems [27], [28] and research in developing algorithms for fusing iUSBL measurements with strapdown navigation sensors (e.g., [29], [30]). iUSBL systems trade complexity on the surface for complexity underwater with the potential advantages of reduced vulnerability to acoustic noise and array motion. Cabled variants permit synchronous operation, obviating the need for bi-directional acoustic transmission, and scale to potentially large numbers of (tethered) underwater assets.

III. Navigation Concept

Fig. 1 illustrates the OWTT-iUSBL concept in the context of multi-AUG operations. A fleet of AUGs operates at depth while an ASV follows on the sea surface. All of the subsea vehicles are equipped with a chip-scale atomic clock (CSAC) that provides a common low-drift time base synchronized to GPS time [31]. At predefined intervals, the ASV transmits an acoustic data packet containing its GPS position along with the time the data packet was transmitted. The accurate time base afforded by CSACs enables each AUG to compare the time it received the data packet with the time it was sent and use this to compute a range. This method of recovering the range is identical to that used in OWTT range-aided navigation. However, this approach differs from OWTT range-aided navigation in that the subsea vehicle is equipped with an acoustic array analogous to conventional USBL that measures the azimuth and elevation angles from the subsea vehicle to the ASV. This measurement (effectively, the position of the ASV relative to the AUG in spherical coordinates) can be transformed to Cartesian coordinates, rotated into the local-level frame using the submerged vehicle's attitude sensor, and finally combined with the transmitted GPS position of the ASV to yield the geo-referenced position of the subsea vehicle with a single acoustic transmission.

Such a system would have important practical distinctions from the iUSBL and range-aided OWTT work reported in the literature and discussed in Section II. Compared to iUSBL,

OWTT-iUSBL eliminates the need for the submerged vehicle to expend the energy necessary to acoustically transmit, and allows all submerged vehicles within range of the ASV to receive position updates at the same time—the proposed system reduces channel utilization by half for a single subsea vehicle and scales to multiple subsea vehicles with no penalty. OWTT-iUSBL also overcomes two limitations of single-source range-only OWTT navigation. First, the method does not *require* fusing the acoustic data with dead-reckoned odometry (e.g., from a DVL/INS) to obtain a position estimate. Instead it provides stand-alone position estimates such as those provided by LBL and conventional USBL systems that can *optionally* be fused with dead-reckoned odometry for improved performance. Second, the method avoids imposing trajectory constraints on the subsea vehicle, surface vehicle, or both, that, when violated, can significantly degrade the solution or render the subsea vehicle position unobservable (Section II). OWTT-iUSBL works for any number of vehicles whose horizontal positions are within approximately one water-depth of the ASV.

IV. Deep-Profiling

OWTT-iUSBL has the potential to enable a new operational paradigm for AUGs—*deep-profiling*, in which the AUG dives to a profile depth and then vertically undulates within a depth band defined by the profile height (Fig. 1). Typically shallow diving AUGs will use subsurface undulating profiles [2], but deep diving AUGs surface after every dive and obtain a GPS fix [3]. Deep-profiling can potentially increase the number of high-value observations on missions where the science dictates a limited portion of the deep water column is of interest. However, deep-profiling comes with the penalty of an increased interval between external navigation aiding from GPS and increased number of pumping cycles (the main source of power consumption) as shown in Fig. 2. OWTT-iUSBL would provide a low-power external navigation solution that would reduce the navigation errors, but we must assess the trade offs of increased power consumption (and thus shortened mission duration) as a result of extra pumping and additional navigation sensors against both increased navigation accuracy and increased near-bottom data collection.

Consider a glider mission focused on observing the ocean in a certain vertical region (Fig. 1) defined by the maximum depth of the profile (the profile depth) and the height above the profile depth that defines the upper boundary of the region (the profile height). We refer to this as the observation region. By defining a set of glider performance parameters (our analysis uses the published values for the Deepglider [15] listed in Table I), we can compute how long a glider will remain in the observation region for two types of trajectories: *conventional* trajectories where the glider dives to the profile depth and then returns to the surface and repeats this cycle for 5 days and *deep-profiling* trajectories where the glider dives to the profile depth and then profiles within the observation region until it surfaces 5 days later.

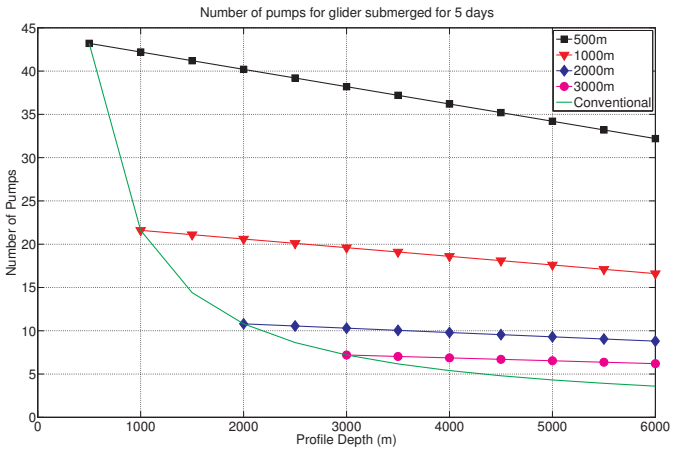

Fig. 2. Number of pumpings for deep-profiling gliders for a hypothetical 5 day dive. Curves are for the different profile heights shown in the legend. The number of profiles for a conventional glider is shown for comparison.

Parameter	**Value**	
Vertical speed, W	0.066 m/s	[15]
Forward speed, U	0.215 m/s	[15]
Hotel power	0.5 W	[15]
Energy Capacity	17MJ	[15]
Dive Buoyancy Volume, Typ.	$\pm$150 cc	n/a†
Pump Flow Rate	1.2 cc/s	[15]

† The volume given is smaller than that originally published in [15] because of recent advances in Deepglider's design (C. Eriksen, personal communication, 10 Aug 2015).

TABLE I
GLIDER ANALYSIS PARAMETERS.

Let R_{dive} denote the ratio of data collected from within the observation region collected by the two gliders over the course of 5 days (multiple cycles for the conventional trajectory; a single dive for the deep-profiling trajectory including multiple cycles within the observation region). Assuming a fixed sample rate, R_{dive} is the ratio of time spent in-band by the two gliders:

$$R_{dive} = \frac{T_{dive} - \frac{2(z-\Delta_z)}{W}}{T_{dive}\frac{\Delta_z}{z}}, \quad (1)$$

where T_{dive} denotes the duration of a single deep-profiling trajectory dive, z and Δ_z the profile depth and height respectively, and W the vertical speed. The numerator gives the time in-band for a glider executing a deep-profiling trajectory—it spends T_{dive} in the observation region minus the transit times required for the initial descent and final ascent. For gliders performing deep-profiling trajectories, the time for a single dive, T_{dive}, is a trade-off between a number of variables including the number of profiles at depth, the frequency at which communications updates are required (only possible on the surface), and, for existing navigation paradigms, the required navigation accuracy. The denominator gives the time within the observation region spent by a glider executing a conventional trajectory (a conventional glider will conduct multiple single profile dives over the period T_{dive} but spend a portion of this time outside the desired depth window).

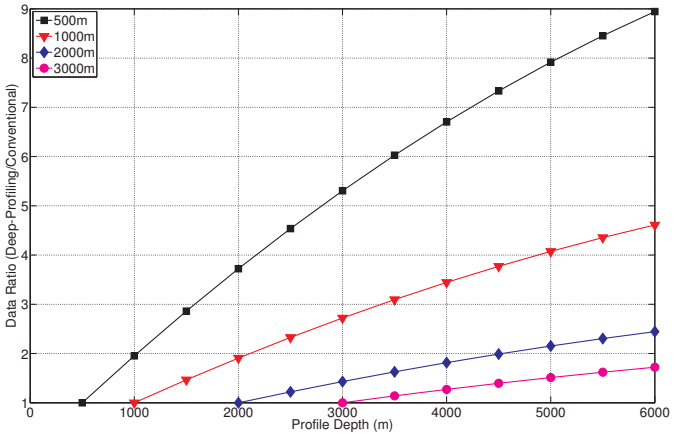

Fig. 3. Inter-surfacing data ratio (R_{dive}, see text) vs. profile depth between a Deepglider surfacing after every profile and a Deepglider equipped executing a deep-profiling trajectory surfacing only every 5 days. Each curve represents a different profile height as indicated in the legend.

For proposes of exposition, we select T_{dive} to be 5 days implying that a deep-profiling glider will surface every 5 days for a communications update and to receive a GPS position fix while a conventional glider will conduct multiple single dive profiles. Fig. 3 shows R_{dive} versus the profile depth for 4 profile heights. As expected, for a fixed time interval the amount of time spent at the desired observational depth increases if the glider can remain submerged for extended periods. For gliders surveying the deep ocean interior, the fixed-interval data ratio increases significantly if the glider only surfaces occasionally as opposed to after every profile.

In the absence of external aiding, the penalty for this increased data-efficiency is increased error in horizontal position (navigation error)—the longer a glider remains submerged, the more navigation error is accumulated. Internal dead-reckoning on gliders, which relies solely on a model of the glider's dynamics and is sensitive to a variety of effects including local currents, rapidly accumulates error without external aiding. While impossible to quantify globally because of the strong dependence on local currents, we will use a value of 13.5% accumulated error per unit distance traveled as a nominal value for the sake of comparison. This statistic is the mean of four glider missions reported in [32] on the basis of comparing GPS locations with estimated position just prior to surfacing. This parameter, combined with the time the glider spends submerged and its forward speed, allow us to estimate the accumulated navigation error for both trajectory types. The deeper a glider dives, the more time spent underwater, the larger the possible accumulated error. A glider executing the conventional trajectory to 6000 m will travel 39 km and accumulate 5.3 km of navigation error between surfacings. A glider executing the 5 day deep-profiling trajectory will travel 93 km and perform correspondingly worse with respect to navigation error, accumulating over 12 km of navigation error between surfacings.

Two issues must be resolved to realize the benefits of increased data return between surfacing intervals that deep-profiling offers: (1) the degradation in dead-reckoned navigational accuracy inherent to prolonged submergence; and (2) the impact on endurance (fewer total dives) of more frequent pumpings and any additional power consumed by navigation enhancements. The next section shows how OWTT-iUSBL addresses the first issue, after which we return to the question of endurance and total data return from a complete deep-profiling mission.

V. Navigation Accuracy

OWTT USBL is subject to essentially the same error sources as conventional (two-way travel time) USBL systems, with the important exception that the accuracy of the surface-to-vehicle slant-range measurement is subject to error growth due to the relative drift of the subsea clock. Table II lists these error sources along with representative error statistics from manufacturer data sheets or other sources as discussed below.

Synchronization: Because the range computed by an OWTT system is dependent on knowledge of the time of the outgoing transmission, synchronization error directly impacts the range estimate. Initial disciplining to a (higher) precision time source is possible only at the start of a mission, after which the frequency of the clock will drift; however, synchronization to GPS is possible on any surfacing such that although the frequency continues to drift, the synchronization error remains small. Ignoring short-term Allan variance and environmental sensitivity, the synchronization error as a function of time is (e.g., [33]):

$$\tilde{T}(t) = \tilde{T}_o + R_o t + \tfrac{1}{2} A t^2 \ , \qquad (2)$$

where $\tilde{T}_o$ denotes the initial synchronization error, R_o the initial frequency error (determines the initial rate at which the clock will gain or lose time), and A denotes the aging rate (subsequent drift in oscillator frequency). For the Microsemi Quantum SA.45s CSAC, application of (2) yields a time synchronization error of no more than 200 ms over the course of an approximately one year long continuous submergence with no opportunity for synchronization. (Performance with better than an order of magnitude *less* drift is reported in early independent assessments of this time standard [31]; our estimate is based on the latest published specifications from the manufacturer and likely extremely conservative especially relative to a well-aged CSAC.) Assuming worst case frequency error (the drift after 1 year without disciplining), surfacing every 5 days for synchronization to GPS (100 ns initial offset) yields a maximum range error of 7 m after 5 days submerged. This value therefore represents a conservative estimate of range error that is applicable to the entire duration of a notional year-long mission with a 5 day surfacing interval.

OWTT USBL: We believe a 0.5° 1σ error in azimuth and elevation is achievable based on the 0.75° 1σ performance reported in [35] for a four-element calibrated transducer head of a design similar to that envisioned for the present application. Initial accuracy is governed by array design and the construction method, improved by tank calibration, and

Error Source	Magnitude	Comments	Power
Synchronization	<5e-11 initial freq.; <1e-8/yr. aging	Microsemi Quantum SA.45s CSAC.	<120 mW (chip only)
OWTT USBL	0.5° azimuth / elevation; <10 m range	5-day surfacing interval, 1σ azimuth / elevation, worst-case range (synchronization error).	350 mW (listen only)
Alignment	0.05° roll/pitch; 0.1° heading	In situ alignment/calibration, Kongsberg HiPAP 500, 1σ [34].	n/a
	0.5° roll/pitch; 1° heading	Mechanical alignment, 1σ.	n/a
Attitude	0.01° roll/pitch, 0.1° heading	iXSea Phins III fiber optic north-seeking gyrocompass, unaided, 1σ.	<20 W
	0.2° roll/pitch, 0.8° heading	Lord Microstrain 3DM-GX4-25, calibrated, "AKF" enabled, 1σ.	550 mW
	2° roll/pitch, 2° heading	PNI SeaTRAX AHRS, calibrated, dynamic attitude, 1σ.	150 mW
Sound Velocity Profile	variable	Affects range and azimuth/elevation estimates (time-of-flight; ray-bending).	n/a

TABLE II
PRINCIPAL ERROR SOURCES FOR A OWTT-IUSBL SYSTEM.

ultimately dependent on signal to noise ratio (SNR) and hence depth. As a point of reference, Hegrenaes et al. [34] quote a 1σ error of 0.12° for the high-end Kongsberg HiPAP 500 USBL system at 20 dB SNR and 0.3° at 0 dB SNR. The range error listed for the proposed system is a conservative estimate based on the worst case synchronization estimate discussed above for a 5-day surfacing interval plus some additional margin.

Alignment: Alignment error refers to the static error in orientation of the USBL array relative to an attitude and heading reference system (AHRS) measuring dynamic vehicle attitude. Conventional high-end commercial systems rely on in situ calibration to a stationary target on the seafloor (in these systems the USBL head and AHRS is mounted on the vessel rather than a subsea vehicle). Alignment accuracy comparable to in situ methods may be possible by utilizing a miniature MEMS-based AHRS and co-locating it with the array (mechanical alignment). We conservatively estimate an order of magnitude worse error for mechanical alignment than the figure quoted in [34] for in situ alignment.

Attitude: Attitude error directly impacts the azimuth and elevation estimates provided by the USBL array. This error source is of particular significance because of the cost and power consumed by accurate heading and attitude sensors. Low power MEMS-based AHRSs rely in part on magnetometers to attain a stable heading measurement, and are consequently subject to bias from hard-iron and soft-iron effects [36], both of which can be calibrated out for a given installation, though the practical considerations associated with carrying out the calibration procedure can be onerous [37]. The table lists a high-end north-seeking fiber optic gyro (FOG) for comparison with two representative MEMS-based sensors: a mid-range unit suitable for integration on LRAUVs, and a low-power unit particularly well-suited to the AUG application. Together the three units span approximately an order of magnitude of attitude error, from $O(0.1^\circ)$ to $O(1^\circ)$, in each of pitch, roll, and heading.

Sound Velocity Profile: The sound velocity profile (SVP) impacts the accuracy of USBL systems in two principal ways: (1) the slant-range estimate is directly affected by multiplication of the measured time-of-flight by the variable sound speed of the water column; (2) sound arriving at the USBL array from other than directly overhead results in ray-bending that affects both range (longer path) and azimuth/elevation (arrival angle). An important characteristic of all USBL systems is that whereas surface-based range-only acoustic aiding methods favor geometries with horizontal offsets on the order of water depth, and therefore subject to ray-bending, USBL systems favor geometries for which the underwater asset is directly below the surface asset. Hegrenaes et al. carried out Monte Carlo simulations of the impact of SVP on USBL error and found the effect negligible [34]. The particular analysis employed considered only shallow water or deep water operation with nearly vertical geometries. As SVP effects are common to all acoustic navigation methods, readily mitigated by occasional surfacing for re-calibration, and have minimal impact for the nearly vertical geometries characteristic of the deep water operations considered here, we have opted to exclude this source of error from our analysis.

Error Propagation: The total single-fix position error represents the compounded effects of these diverse error sources. The geometry of iUSBL is analogous to conventional USBL. The position of the ASV is provided to the subsea USBL system via telemetry; therefore, the georeferenced subsea position of the vehicle is the georeferenced position of the ASV offset by the relative position of the ASV in a local-level North-East-Down (NED) frame attached to the subsea vehicle. We are concerned with the impacts of the error sources in Table II on the relative position. The relative position as measured by iUSBL can be expressed in simplified form as

$$ {}^{n}\mathbf{p}_{\mathrm{ASV}} = {}^{n}_{v}\mathbf{R}\,{}^{v}_{u}\mathbf{R}\,{}^{u}\mathbf{p}_{\mathrm{ASV}}\,, \tag{3} $$

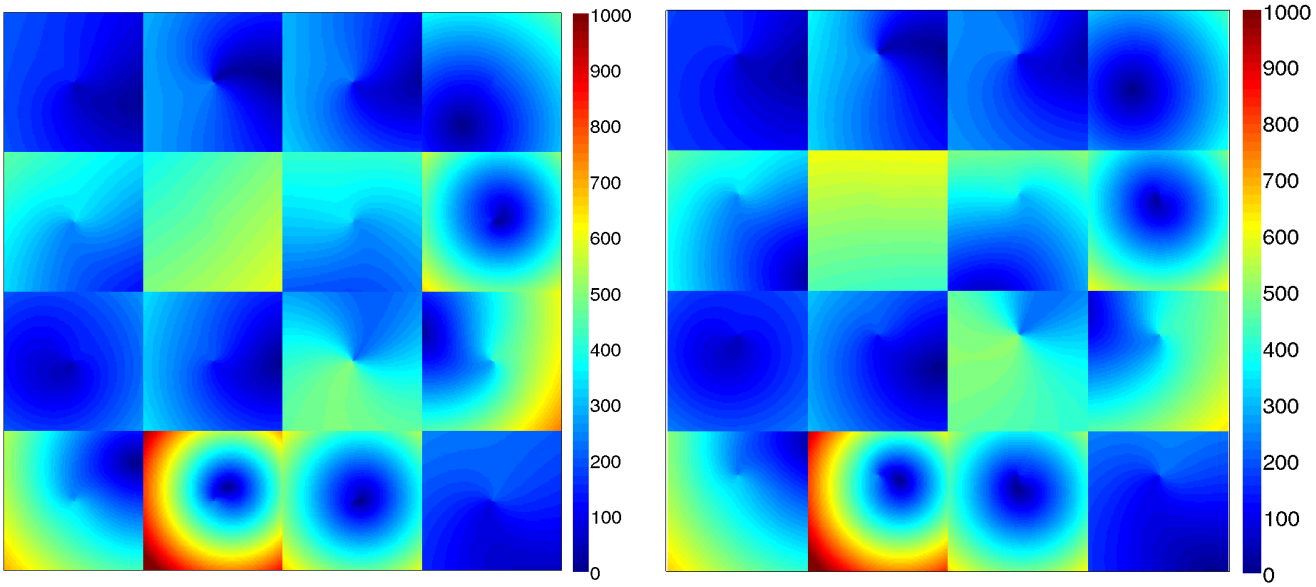

Fig. 4. Simulated realizations of the horizontal component of position error for a mechanically-aligned OWTT-iUSBL system with a PNI SeaTRAX AHRS plotted as a function of true horizontal position for an underwater vehicle at 5000 m depth. Each tile is a single realization, 10,000 m on a side, with the ASV located at the center of the tile. The color represents the magnitude (in meters) of the horizontal position error. Left: 16 realizations for an underwater vehicle flying level. Right: 16 realizations for an AUG pitched at 20°. Corresponding tiles between the two plots have the same set of randomly-generated measurement errors applied—the differences are due only to true vehicle pitch.

where the sub/superscripts n, v, and u denote the local-level, vehicle and iUSBL transducer frames, respectively. The position vector ${}^{u}\mathbf{p}_{\mathrm{ASV}}$ denotes the position of the ASV in the coordinate frame of the iUSBL transducer, ${}^{u}_{v}\mathbf{R}$ the fixed alignment between the iUSBL transducer and the subsea vehicle's attitude sensor and ${}^{n}_{v}\mathbf{R}$ the attitude measured by that sensor, and ${}^{n}\mathbf{p}_{\mathrm{ASV}}$ the position of the ASV in the local-level frame. Equation (3) assumes the origins of all three frames are coincident and affixed the the subsea vehicle. This simplification is possible because small translational offsets between frames represent negligible error sources in comparison to angular errors, which are effectively amplified by the range between the subsea vehicle and ASV.

Position data from a USBL system is expressed most naturally in terms of spherical coordinates as range, Γ, azimuth, α, and elevation, γ:

$$ {}^{u}\mathbf{p}_{\mathrm{ASV}} = \Gamma \begin{bmatrix} \cos\gamma\cos\alpha \\ \cos\gamma\sin\alpha \\ \sin\gamma \end{bmatrix} . \tag{4} $$

In total there are 5 time-varying angular measurements plus 3 fixed angles and one distance, Γ, that are subject to measurement or calibration error (plus a negligible additive position error from the GPS position of the ASV itself).

Equation (3) can be used to examine the effects, individual or compounded, of each error source. In general, the impact of each error source is dependent on the true vehicle position, attitude, and array/AHRS alignment, or equivalently on true values for ${}^{n}\mathbf{p}_{\mathrm{ASV}}$, ${}^{n}_{v}\mathbf{R}$, and ${}^{n}_{n}\mathbf{R}$, respectively. We restrict our attention to the practically motivated situation of identity alignment, a vehicle rolled at zero degrees and either flying level or pitched at a typical glide angle of 20°. In what follows the vehicle is also assumed, without further loss of generality, to be headed due north. The impact of measurement errors in the terms of (3) can then be visualized as a function of true position ${}^{n}\mathbf{p}_{\mathrm{ASV}}$. To generate the visualizations in Fig. 4 we inverted (3) for the true iUSBL azimuth elevation and range, then generated a corrupted position measurement by adding random measurement errors to each of the 8 angles and 1 range in (3). Each tile in Fig. 4 illustrates an error surface that results from a different randomly generated set of 9 measurement errors. The region directly beneath the ASV (the center of each tile) rarely exhibits large errors, in contrast to the edges at approximately 1 water depth horizontal distance from the ASV. A discontinuity is apparent directly beneath the ASV in the level flight case and offset to the north in the pitched case.

The error surface realizations of Fig. 4 are useful for building intuition but lack the simplicity of an error budget. Following the procedure for a conventional USBL system outlined in [34], we derived a total error budget from the data in Tab. II using standard 1st order linearized uncertainty propagation applied to (3) followed by the assumption of independent error sources to arrive at an estimate of the standard deviation for total horizontal position error via the variance formula (eq. (2.10) in [38]). Linearized about a nominal vehicle orientation of 0° pitch and roll, variance propagation applied to (3) yields a radially symmetric error that grows with distance from the ASV. Radial symmetry breaks down for non-zero pitch; however, comparing the panels of Fig. 4 suggests that the magnitude of the horizontal position error is not dramatically different between a level vehicle and one pitched as much as 20°—relative position dominates. This allows the

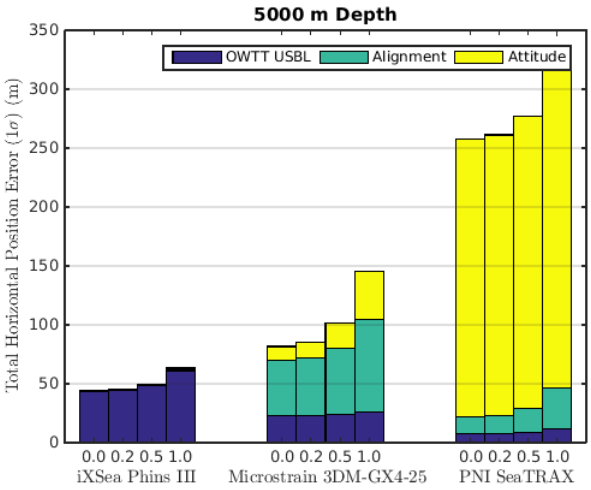

Fig. 5. Single-fix error budget (1σ) for an underwater vehicle flying level at 5000 m depth. Each group of four bars represents a vehicle equipped with a particular AHRS (left-to-right, in order of decreasing precision and power consumption: iXSea Octans or unaided Phins north-seeking FOG; Lord Microstrain 3DM-GX4-25, and PNI Sensor Corporation SeaTRAX). Each bar within a group is labeled with horizontal range of the vehicle from the ASV, expressed as a fraction of total water depth. Each bar is split according to the percentage of the *variance* explained by each source of error.

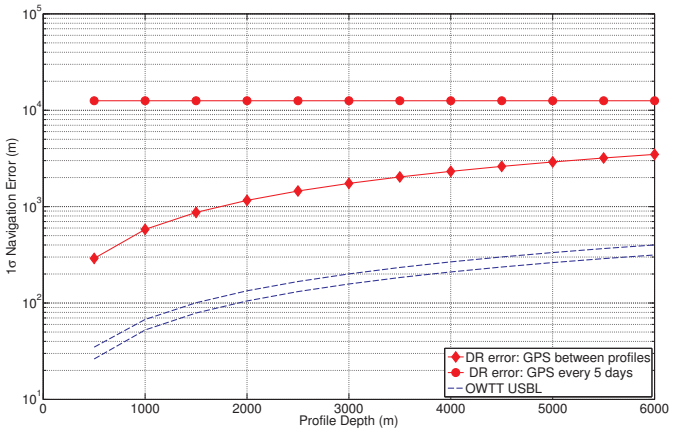

Fig. 6. 1σ horizontal position error for AUGs reliant on dead-reckoning between surfacing for GPS (red) compared with a notional low-power OWTT-iUSBL system (blue) as a function of profile depth. The red diamonds show the accumulated navigation error just prior to surfacing for a glider executing a single profile to depth. The red circles show the accumulated navigation error for an AUG after 5 days submerged without GPS. The dashed blue curves are estimates of the performance attained by a OWTT-iUSBL system for an AUG directly beneath (lower curve) and displaced horizontally by one water-depth (upper curve) from a surface beacon.

error budget to be concisely summarized as a function of radial distance from the ASV.

Fig. 5 presents the error budget for three representative applications, a high-speed survey-class AUV equipped with a high-end north-seeking FOG; a vehicle equipped with a mid-grade MEMS-based attitude sensor suitable for use on LRAUVs and a low-power MEMS-based attitude sensor with extremely low power (0.3 mW) sleep mode suitable for use on oceanographic gliders especially if duty-cycled. Like all USBL systems, the proposed system provides a complete 3-degree of freedom position estimate; however, depth can be measured to better accuracy by sensors with modest power requirements and already carried by the vehicle platforms we anticipate will benefit most from the technology. The error budget of Fig. 5 therefore considers only the horizontal components of position error associated with the system. The figure illustrates some important aspects of these notional systems: (1) attitude error dominates for low-power platforms; and (2) errors are smallest directly beneath the surface beacon. The aspects are particularly important in light of (1) the rapid progress in terms of power, size and accuracy of MEMS-based AHRSs; and (2) acoustic communication favors use of a vertical channel.

Figure 6 compares the navigation performance of a deep-profiling AUG equipped with OWTT-iUSBL versus a deep-profiling AUG dead-reckoning between surfacings and an AUG executing a conventional profile. The OWTT-iUSBL curves were generated for a mechanically aligned system and the lowest-power AHRS option. Note that the y-axis is logarithmic—the system would deliver a 1–2 order of magnitude improvement in navigation for depths as shallow as 500 m.

VI. Endurance Analysis

Our navigation analysis shows that an AUG equipped with OWTT-iUSBL could possess significantly improved navigational performance while being largely relieved of the need to surface for GPS. For example, a glider diving to 3000 m would have a 1σ navigation accuracy of 155 m if the surface beacon were directly overhead and 196 m if the surface beacon were a water depth away (i.e., 3000 m). Similarly, a glider diving to 6000 m would have 1σ navigation accuracy ranging from 310–392 m. This represents a significant improvement over the current paradigm and, from a navigation prospective, enables deep-profiling missions. However, deep-profiling missions incur two penalties with respect to the glider's overall energy budget and thus endurance: *(1)* the power consumption of the OWTT-iUSBL and *(2)* the additional energy consumed by the pump for the increased number of profiles.

This section studies deep-profiling missions from an energy prospective. Our analysis considers three components of the glider's power budget: *(i)* hotel load (e.g., the host computer), *(ii)* the OWTT-iUSBL system, and *(iii)* propulsion. On the Deepgliders, power for the science sensors is provided by a dedicated 4.3MJ battery (as opposed to the main 17MJ battery) [15], thus we ignore science sensor power. The hotel load for a Deepglider is $P_{hotel} = 0.5$ W.

Navigation Power: Three components contribute to the OWTT-iUSBL power budget: the CSAC, AHRS, and acoustic modem electronics (receive only). The CSAC consumes 0.15 W including a small allowance for electronics auxiliary to the chip itself, and the remaining components 0.35 W, and 0.15 W, respectively. The CSAC must always be on; however the AHRS and acoustic modem electronics can be duty-cycled—powered down most of the time and then, using

the CSAC as a timing device, be powered on when the glider is scheduled to receive an acoustic modem message. For this analysis, we assume a navigation update occurs every 4 hours (the same update rate used in prior glider experiments employing external acoustic aiding [17], [18]) and that the AHRS and modem electronics are otherwise powered down.

Propulsion Power: Gliders are propelled by changes in buoyancy. On Deepglider a high pressure pump moves oil between an internal reservoir and an external bladder exposed to ambient pressure to alter its effective displacement and thus alter its buoyancy. The power required to effect a change from negative to positive buoyancy at depth is a function of the ambient pressure—we extrapolated the electrical pump power from Fig. 3 in [3] to get a pump power formula of $P_{pump}(z) = (0.016z + 14)$ W. (During the change from positive to negative buoyancy, ambient pressure is used to push oil from the bladder back into the internal reservoir, a process referred to as bleeding.) The pump energy, $E_{pump}(z)$, is the pump power multiplied by the time required for the pump to displace the dive buoyancy volume. Recent work with Deepgliders uses a dive buoyancy volume of ± 150 cc (C. Eriksen, personal communication, 10 Aug 2015); pumping at 1.2 cc/s [15] this results in a pumping time of 250 s. The propulsion energy required for a fixed time interval is then the number of profiles executed during that time interval multiplied by $E_{pump}(z)$.

The total energy budget for a glider executing a conventional trajectory over a fixed time interval, T_{dive}, is

$$E_{dive,o} = T_{dive}P_{hotel} + \frac{T_{dive}}{\frac{2z}{W}}E_{pump}(z) \ , \tag{5}$$

where again W is the glider's vertical speed. The energy consumed by a OWTT-iUSBL-equipped glider executing a deep-profiling trajectory over the same interval is

$$E_{dive} = E_{nav} + T_{dive}P_{hotel} + \frac{T_{dive} - \frac{2(z-\Delta_z)}{W}}{\frac{2\Delta_z}{W}}E_{pump}(z) \tag{6}$$

where E_{nav} is consumed by the OWTT-iUSBL system. The terms multiplying the per-profile pump energy E_{pump} are the number of negative-to-positive buoyancy changes executed over the fixed time interval T_{dive} for either trajectory variant (Fig. 2).

Knowing the energy per fixed interval for both the conventional and deep-profiling trajectories, we can then divide the main battery capacity of a Deepglider (17MJ [15]) to get the number of dives that can be completed using each glider trajectory during a deployment. This provides both the *endurance* of the glider (the number of intervals multiplied by the interval length) as well as the *number of observations* each glider trajectory obtains in the desired depth window during the entire deployment. As in Fig. 3, we compute a data ratio which is the number of observations obtained in the desired depth window for the deep-profiling trajectory divided by those for a conventional trajectory.

Fig. 7 shows the endurance (left panel) and data ratio (right panel) for our analysis. As expected, a OWTT-iUSBL-equipped glider executing the deep-profiling trajectory has a reduced endurance; however, the data ratio still favors the deep-profiling glider for a large range of profile depth and heights (i.e., $R>1$). The increased power consumption of the OWTT-iUSBL glider is mitigated by the time saved not having to ascend after each profile for a GPS fix. For example, a OWTT-iUSBL glider doing 1000 m high profiles at a profile depth of 3000 m will spend 52% more time within the observation region than a glider that ascends after each profile even though its endurance is reduced to 145 days (compared to 265 days for a conventional trajectory). These increased observations are in addition to the fact that OWTT-iUSBL glider would receive external navigation updates every four hours that constrain its position to within 200 m (as opposed to almost 2 km of error accumulated by a conventional glider doing a 3000 m profile). In fact, increasing the OWTT-iUSBL update rate to 10 minutes has a marginal impact on endurance—a OWTT-iUSBL glider doing 1000 m high profiles at a profile depth of 3000 m will spend 49% more time within the observation region than a conventional glider and have an endurance of a 143 days.

VII. Conclusion

OWTT-iUSBL has the potential to overcome the existing obstacles of size, cost and power that preclude routine accurate externally-aided navigation in the ocean interior. This paper reported a feasibility and performance analysis for a notional OWTT-iUSBL system for use on a deep-diving AUG, suggesting a putative 1σ horizontal position accuracy of 30–300 m depending primarily on the attitude sensor used, the depth of the AUV or AUG, and the horizontal distance between the ASV and the submerged vehicle. Using extant low-power attitude sensors compatible with the restrictive power-budget on deep-diving AUGs, a practically realizable OWTT-iUSBL system could provide a navigational accuracy 1–2 orders of magnitude superior to that presently achievable using periodic ascents to acquire GPS. In addition, while the notional system would uniformly improve the navigation of deep-diving AUGs, for scenarios in which only a portion of the deep water column is of interest, it would also yield more data *despite* reducing overall vehicle endurance because the AUG expends more of its energy within the depth band of interest instead of on transits to the surface.

Our analyses suggest OWTT-iUSBL could significantly broaden the scope of missions practically achievable by deep-diving AUGs. Near term, deep-diving AUGs could perform ridge-segment-scale hydrothermal vent surveys and aid in the characterization localized deep water flows over sills. Looking farther ahead, an OWTT-iUSBL system could enable teams of LRAUVs and an attending ASV to undertake basin-scale surveys of the seafloor with improved navigation and a vastly reduced need to surface.

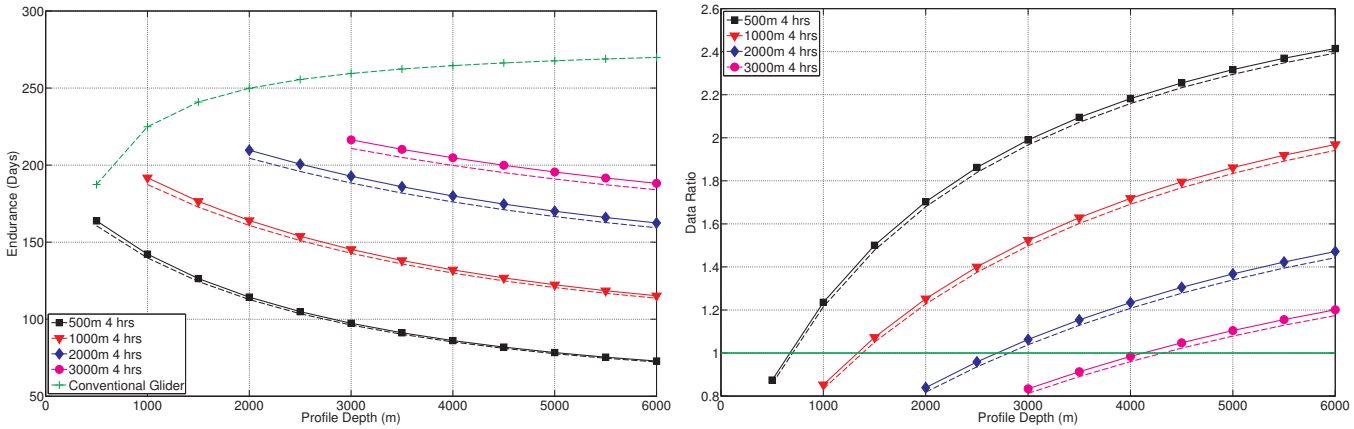

Fig. 7. *Left:* Endurance of gliders performing conventional trajectories as well as deep-profiling trajectories. For the deep-profiling trajectories, four different profile heights are shown. Solid lines are for a OWTT-iUSBL update rate of 4 hours; the dashed lines are for a 10 minute update rate. *Right:* The data ratios for an entire glider deployment. A data ratio greater than 1 indicates that the deep-profiling trajectory obtains more measurements within the desired depth window then a conventional trajectory despite the shorter deployment length. Again, four different profile heights are shown for the the deep-profiling trajectories, and solid lines indicate a OWTT-iUSBL update rate of 4 hours and dashed lines a 10 minute update rate.

ACKNOWLEDGMENTS

Louis L. Whitcomb and Ryan M. Eustice introduced the authors to the transformative potential of low-power high-precision clocks in the context of underwater navigation and inverted USBL in particular. Their original conceptualization inspired the feasibility analyses reported in this paper. Discussions with Christopher R. German helped to frame the scientific need for precisely-navigated long-endurance deep-water survey.

REFERENCES

[1] H. Stommel, "The Slocum mission," *Oceanography*, vol. 2, no. 1, pp. 22–25, 1989.

[2] D. Webb, P. Simonetti, and C. Jones, "SLOCUM: an underwater glider propelled by environmental energy," *IEEE J. Oceanic Eng.*, vol. 26, no. 4, pp. 447–452, Oct 2001.

[3] C. Eriksen, T. Osse, R. Light, T. Wen, T. Lehman, P. Sabin, J. Ballard, and A. Chiodi, "Seaglider: a long-range autonomous underwater vehicle for oceanographic research," *IEEE Journal of Oceanic Engineering*, vol. 26, no. 4, pp. 424–436, 2001.

[4] A. M. Bradley and D. R. Yoerger, "Design and testing of the autonomous benthic explorer," in *Proceedings of AUVS '93*, 1993.

[5] B. Allen, R. Stokey, N. Forrester, R. Goldsborough, M. Purcell, and C. von Alt, "REMUS: a small, low cost AUV; system description, field trials and performance results," in *Proceedings of IEEE/MTS Oceans Conference*, vol. 2, October 1997, pp. 994–1000.

[6] R. Marthiniussen, K. Vestgard, R. A. Klepaker, and N. Storkersen, "HUGIN-AUV concept and operational experiences to date," in *Proc. IEEE/MTS OCEANS Conf. Exhib.*, vol. 2, Kobe, Japan, Nov. 2004, pp. 846–850.

[7] G. Griffiths, "Autosub under ice," *Ingenia*, vol. 22, pp. 30–32, 2005.

[8] R. Stokey, A. Roup, C. von Alt, B. Allen, N. Forrester, T. Austin, R. Goldsborough, M. Purcell, F. Jaffre, G. Packard, and A. Kukulya, "Development of the REMUS 600 autonomous underwater vehicle," in *Proceedings of IEEE/MTS Oceans Conference*, 2005, pp. 1301–1304.

[9] K. Sharp and R. White, "More tools in the toolbox: The naval oceanographic office's remote environmental monitoring units (remus) 6000 AUV, year = 2008, month = Sept, pages = 1–4," in *Proc. IEEE/MTS OCEANS Conf. Exhib.*

[10] M. Furlong, S. McPhail, and P. Stevenson, "A concept design for an ultra-long-range survey class AUV," in *Proc. IEEE OCEANS-Europe Conf. Exhib.*, Aberdeen, June 2007, pp. 1–6.

[11] J. Bellingham, B. Hobson, M. A. Godin, B. Kieft, J. Erikson, R. McEwen, C. Kecy, Y. Z. T. Hoover, and E. Mellinger, "A small, long-range AUV with flexible speed and payload," in *Ocean Sciences Meeting*, 2010.

[12] J. Kinsey, D. Yoerger, M. Jakuba, R. Camilli, C. R. Fisher, and C. German, "Assessing the Deepwater Horizon oil spill with the Sentry autonomous underwater vehicle," in *Proc. IEEE/RSJ Intl. Conf. Intell. Robots Systems*, Sept 2011, pp. 261–267.

[13] B. Curry, C. M. Lee, B. Petrie, R. E. Moritz, and R. Kwok, "Multi-year volume, liquid freshwater, and sea ice transports through Davis Strait, 2004-10," *J. Phys. Oceanogr.*, vol. 44, pp. 1244–1266, 2014.

[14] R. E. Todd, D. L. Rudnick, M. R. Mazloff, R. E. Davis, and B. D. Cornuelle, "Poleward flows in the southern California Current system: Glider observations and numerical simulation," *Journal of Geophysical Research: Oceans*, vol. 116, no. C2, pp. 2156–2202, 2011.

[15] T. J. Osse and C. C. Eriksen, "The Deepglider: A full ocean depth glider for oceanographic research," in *Proc. IEEE/MTS OCEANS Conf. Exhib.*, Vancouver, BC, Sept 2007, pp. 1–12.

[16] M. E. Furlong, D. Paxton, P. Stevenson, M. Pebody, S. D. McPhail, and J. Perrett, "Autosub long range: A long range deep diving AUV for ocean monitoring," in *Autonomous Underwater Vehicles (AUV), 2012 IEEE/OES*, September 2012, pp. 1 –7.

[17] S. E. Webster, C. M. Lee, and J. I. Gobat, "Preliminary results in under-ice acoustic navigation for Seagliders in Davis Strait," in *Proc. IEEE/MTS OCEANS Conf. Exhib.*, St. John's, Sept 2014, pp. 1–5.

[18] S. E. Webster, L. E. Freitag, C. M. Lee, and J. I. Gobat, "Towards real-time under-ice acoustic navigation at mesoscale ranges," in *Proc. IEEE Intl. Conf. Robot. Auto.*, Seattle, WA, May 2015, pp. 1–8.

[19] R. M. Eustice, H. Singh, and L. L. Whitcomb, "Synchronous-clock, one-way-travel-time acoustic navigation for underwater vehicles," *Journal of Field Robotics*, vol. 28, no. 1, SI, pp. 121–136, Jan-Feb 2011.

[20] J. Kinsey, M. Jakuba, and C. German, "A long term vision for long-range ship-free deep ocean operations: persistent presence through coordination of autonomous surface vehicles and autonomous underwater vehicles," in *Workshop on Marine Robotics and Applications. Looking into the Crystal Ball: 20 years hence in Marine Robotics*, 2013.

[21] S. Webster, R. Eustice, H. Singh, and L. Whitcomb, "Advances in single-beacon one-way-travel-time acoustic navigation for underwater vehicles," *The International Journal of Robotics Research*, vol. 31, no. 8, pp. 935–950, 2012.

[22] M. F. Fallon, G. Papadopoulos, J. J. Leonard, and N. M. Patrikalakis, "Cooperative AUV navigation using a single maneuvering surface craft," *Intl. J. Robotics Research*, vol. 29, no. 12, pp. 1461–1474, Oct 2010.

[23] A. Gadre and D. Stilwell, "A complete solution to underwater navigation in the presence of unknown currents based on range measurements from a single location," in *Proc. IEEE/RSJ Intl. Conf. Intell. Robots Systems*, 2005, pp. 1420–1425.

[24] P. Baccou and B. Jouvencel, "Simulation results, post-processing experimentations and comparisons results for navigation, homing and multiple vehicles operations with a new positioning method using on transponder," in *IEEE International Conference on Intelligent Robots and Systems*, vol. 1, Las Vegas, NV, United States, Oct. 2003, pp. 811–817.

[25] T. L. Song, "Observability of target tracking with range-only measurements," *Oceanic Engineering, IEEE Journal of*, vol. 24, no. 3, pp. 383–387, 1999.

[26] A. P. Scherbatyuk, "The AUV positioning using ranges from one transponder LBL," in *Proc. IEEE/MTS OCEANS Conf. Exhib.*, vol. 3, San Diego, CA, 1995, pp. 1620–1623.

[27] K. Vickery, "Acoustic positioning systems - new concepts: The future," in *Proceedings of the IEEE Symposium on Autonomous Underwater Vehicle Technology*, Cambridge, MA, USA, Aug. 1998, pp. 103–110.

[28] T. Hiller, A. Steingrimsson, and R. Melvin, "Expanding the small auv mission envelope; longer, deeper & more accurate," in *Autonomous Underwater Vehicles (AUV), 2012 IEEE/OES*. IEEE, 2012, pp. 1–4.

[29] P. Batista, C. Silvestre, and P. Oliveira, "Gas tightly coupled lbl/usbl position and velocity filter for underwater vehicles," in *Control Conference (ECC), 2013 European*. IEEE, 2013, pp. 2982–2987.

[30] M. Morgado, P. Oliveira, and C. Silvestre, "Tightly coupled ultrashort baseline and inertial navigation system for underwater vehicles: An experimental validation," *Journal of Field Robotics*, vol. 30, no. 1, pp. 142–170, 2013.

[31] A. Gardner and J. Collins, "Advancements in high-performance timing for long term underwater experiments: A comparison of chip scale atomic clocks to traditional microprocessor-compensated crystal oscillators," in *Oceans, 2012*, Oct 2012, pp. 1–8.

[32] B. Claus, R. Bachmayer, and C. Williams, "Development of an auxiliary propulsion module for an autonomous underwater glider," *Proceedings of the Institution of Mechanical Engineers, Part M: Journal of Engineering for the Maritime Environment*, vol. 224, no. 4, pp. 255–266, 2010.

[33] J. R. Vig, "Quartz crystal resonators and oscillators for frequency control and timing: A tutorial," US Army Electronics Technology and Devices Laboratory, Fort Monmouth, NJ, USA, Tech. Rep., Oct. 1991.

[34] O. Hegrenaes, T. Sabo, P. E. Hagen, and B. Jalving, "Horizontal mapping accuracy in hydrographic AUV surveys," in *Autonomous Underwater Vehicles (AUV), 2010 IEEE/OES*. IEEE, 2010, pp. 1–13.

[35] F. M. Jaffré, T. C. Austin, B. G. Allen, R. Stokey, and C. J. Von Alt, "Ultra short baseline acoustic receiver/processor," in *Proc. IEEE OCEANS-Europe Conf. Exhib.*, vol. 2, 2005, pp. 1382–1385.

[36] M. J. Caruso, "Applications of magnetic sensors for low cost compass systems," in *Position Location and Navigation Symposium, IEEE 2000*, Mar. 2000, pp. 177–184.

[37] M. V. Jakuba, O. Pizarro, and S. B. Williams, "High resolution, consistent navigation and 3D optical reconstructions from AUVs using magnetic compasses and pressure-based depth sensors," in *Proc. IEEE/MTS OCEANS Conf. Exhib.*, Sydney, 2010, pp. 1–9.

[38] H. Ku, "Notes on the use of propagation of error formulas," *Journal of Research of the National Bureau of Standards*, vol. 70, no. 4, 1966.